Stanford Exploration Project, Report 94, November 11, 1997, pages 1–299

Stanford Exploration Project, Report 94, November 11, 1997, pages 1–299

Prestack time migration for anisotropic media

Tariq Alkhalifah[1]

keywords: *anisotropy, prestack migration*

ABSTRACT

Prestack phase-shift migration is implemented by evaluating the offset-wavenumber (k_h) integral using the stationary-phase method. Thus, the stationary point along k_h must be calculated prior to applying the phase shift. This type of implementation allows for migration of separate offsets, as opposed to migration of the whole prestack data when using the original formulas. For zero-offset data, the stationary point (k_h=0) is known in advance, and, therefore, the phase-shift migration can be implemented directly. For non-zero-offset data, we first evaluate k_h that corresponds to the stationary point solution either numerically or through analytical approximations. The insensitivity of the phase to k_h around the stationary point solution (its maximum) implies that even an imperfect k_h obtained analytically can go a long way to getting an accurate image. In transversely isotropic (TI) media, the analytical solutions of the stationary point (k_h) include more approximations than those corresponding to isotropic media (i.e., approximations corresponding to weaker anisotropy). Nevertheless, the resultant equations, obtained using Shanks transforms, produce accurate migration signatures for strong anisotropy ($\eta \approx$0.3) and even large offset-to-depth ratios (>2). The analytical solutions are particularly accurate in predicting the non-hyperbolic moveout behavior associated with anisotropic media, a key ingredient to performing an accurate non-hyperbolic moveout inversion for strongly anisotropic media. Although the prestack correction achieved using the phase-shift method can also be obtained using a cascade of normal-moveout correction, dip-moveout (DMO) correction, and zero-offset time migration, the prestack approach can handle sharper velocity models more efficiently. In addition, the resulting operator is *cleaner* than that obtained from the DMO method. Synthetic and field data applications of the proposed prestack migration demonstrate its usefulness.

[1]**email:** tariq@sep.stanford.edu

INTRODUCTION

Zero-offset phase-shift method of migration (Gazdag, 1978) is a robust and efficient way of seismic imaging. Gazdag migration ranks second only to Stolt (1978) in efficiency, and it can exactly (within the limit of ray theory) handle the kinematics of migrating data from $v(z)$ media, whereas Stolt migration resorts to approximations to handle $v(z)$ variations of velocity. Gazdag migration, with some modification (Gazdag and Sguazzero, 1984; Stoffa and Fokkema, 1990) can approximately handle smooth lateral velocity variation.

Extending phase-shift migration to treat prestack data is accomplished by using the double-square-root (DSR) equation of Yilmaz (1979). Its implementation in practice, however, is rare, if non existent; using the DSR equation in its original form requires that all offsets and common-midpoint (CMP) data be downward continued simultaneously. The output of such a prestack migration process is a stacked section that does not hold any explicit velocity information, or otherwise, some notable artifacts will occur during integration of the offset-wavenumber axis due to the sparseness in its sampling. Popovici (1995) showed that such artifacts can be avoided by subsampling the offset-wavenumber axis so that the integration range does not include evanescent waves. He also developed a technique to reserve the full complement of offsets free of artifacts after migration; he devised a method to downward continue separate offsets by evaluating the offset-wavenumber integral with the stationary-phase method. Determining the stationary point required solving a six-order polynomial which Popovici elected to avoid doing analytically. His numerical solutions of the stationary points, according to his assessment, were relatively expensive, because they required an additional integration.

In this paper, I discuss the stationary point solution associated with evaluating the offset-wavenumber integral, and show efficient numerical and approximate analytical solutions. The numerical implementation of the separate-offset phase-shift migration is based on tabulating the stationary point solutions. It is efficient enough to use in practice, especially for migrating transversely isotropic media. I also show analytical approximations of the stationary-point solution in both isotropic and anisotropic homogeneous media. Applications to synthetic and real data follow.

ANISOTROPIC MEDIA PARAMETERIZATION

Here, I consider the simplest and probably most practical anisotropic model, that is, a transversely isotropic (TI) medium with a vertical symmetry axis. Such a medium is regarded in the anisotropic world with the same importance that $v(z)$ velocity variation has in the inhomogeneous world. Although more complicated kinds of anisotropies can exist (i.e., orthrohombic anisotropy), the large amount of shales present in the subsurface implies that the TI model has the most influence on P-wave data (Banik, 1984).

In homogeneous transversely isotropic media with a vertical symmetry axis (VTI media), P- and SV-waves [2] can be described by the vertical velocities V_{P0} and V_{S0} of P- and S-waves, respectively, and two dimensionless parameters ϵ and δ (Thomsen, 1986).

$$\epsilon \equiv \frac{c_{11} - c_{33}}{2c_{33}},$$

$$\delta \equiv \frac{(c_{13} + c_{44})^2 - (c_{33} - c_{44})^2}{2c_{33}(c_{33} - c_{44})}.$$

Tsvankin (1995) and Alkhalifah (1997c) demonstrated that P-wave velocity and traveltime are practically independent of V_{S0}, even for strong anisotropy. This implies that, for practical purposes, P-wave kinematic signatures can be considered as a function of just three parameters: V_{P0}, δ, and ϵ.

Alkhalifah and Tsvankin (1995) further demonstrated that a new representation in terms of just *two* parameters is sufficient for performing all time-related processing, such as normal moveout correction (including non-hyperbolic moveout correction, if necessary), dip-moveout correction, and prestack and post-stack time migration. These two parameters are the normal-moveout velocity for a horizontal reflector

$$V_{\rm nmo}(0) = V_{p0}\sqrt{1 + 2\delta}\,, \tag{1}$$

and the anisotropy coefficient η,

$$\eta \equiv 0.5\left(\frac{V_h^2}{V_{\rm nmo}^2(0)} - 1\right) = \frac{\epsilon - \delta}{1 + 2\delta}\,, \tag{2}$$

where V_h is the horizontal velocity. Instead of $V_{\rm nmo}$, I will use v to represent the interval NMO velocity in both isotropic and TI media.

Moreover, Alkhalifah and Tsvankin (1995) further show that these two parameters, η and $V_{\rm nmo}(0)$, are obtainable solely from surface seismic P-wave data: specifically, from estimates of stacking velocity for reflections from interfaces having two distinct dips. These two parameters can also be resolved by examining the behavior of moveout at far offsets (Alkhalifah, 1997b). The third parameter, V_{P0}, is needed for time-to-depth conversion only. The two-parameter representation and inversion also holds in $v(z)$ media (Alkhalifah, 1997a). For that situation, these two parameters are expressed in terms of the vertical time τ.

Because the main assumption in the new parameterization is that the data remain in the time rather than depth domain, the post-stack migration considered here is primarily a time one[3].

[2] I omit the qualifiers in "quasi-P-wave" and "quasi-SV-wave" for brevity

[3] Implications where depth migration is a necessity will be discussed in a follow-up paper

TIME MIGRATION

Fourier-domain implementations of migration require that the medium to be laterally homogeneous (excluding some approximations used to handle smooth lateral velocity variation). However, this inherent limitation of time-migration results in implementations of migration in the Fourier domain, that are efficient. In addition, the assumption of lateral homogeneity allows, as mentioned above, for the two-parameter representation of P-waves in VTI media. Likely, through the combined action of gravity and sedimentation, velocity variation with depth represents the most important first-order inhomogeneity in the earth. This is one reason why time migration works well in so many places. The reader familiar with zero-offset time migration (Gazdag, 1978), and Popovici (1993) separate offset migration may prefer to skip this section, which is a summary of both methods. This section also introduces some notations used throughout this paper.

Zero-offset phase-shift migration

Gazdag's (1978) phase-shift method for depth extrapolation of a seismic wave-field in the frequency-wavenumber (ω, k_x) domain is given by

$$W(\omega, k_x, z) = W(\omega, k_x, z=0)\, A(k_x/\omega, z)\, e^{i2\omega \int_0^z d\zeta\, \frac{\cos\theta(k_x/\omega, \zeta)}{v(\zeta)}} \tag{3}$$

(Hale, 1992), where W is the wave-field, ω is the angular frequency, k_x is the horizontal component of the wave number, z is the depth, and $\theta(p_x, z)$ is the angle defined, for isotropic media, by

$$\sin\theta(p_x, z) = v(z) p_x,$$

where p_x is the horizontal component of slowness. $A(p_x, z)$ is an amplitude factor that corrects for the $v(z)$ influence and is often omitted, partially because it goes to infinity as z approaches the turning point, that depth where $\theta(p_x, z) = \pm 90$ degrees. This erroneous infinite amplitude is similar to that encountered when performing Kirchhoff migration with WKBJ amplitudes determined by Cartesian-coordinate ray tracing (non-dynamic). I will also omit this amplitude factor in the rest of this paper.

Equation (3) is the WKBJ solution (e.g., Aki and Richards, 1980, page 416) of the differential equation,

$$\frac{d^2W}{dz^2} + \left[\frac{\omega^2}{v^2(z)} - k_x^2\right] W = 0,$$

which is the wave equation, expressed in the frequency-wavenumber domain (the Helmholtz's equation).

For migration of zero-offset seismic data $f(t, x)$, we identify $W(\omega, k_x, z=0)$ as the Fourier transformed data $F(\omega, k_x)$ recorded at the earth's surface ($z = 0$). Inverse

Fourier transformation of equation (3) from wavenumber k_x to distance x gives

$$W(\omega, x, z) = \frac{1}{2\pi} \int dk_x \, e^{i2\omega \int_0^z d\zeta \, \frac{\cos\theta(k_x/\omega,\zeta)}{v(\zeta)} + ik_x x} \, F(\omega, k_x), \tag{4}$$

and then evaluation of the inverse Fourier transformation from frequency ω to time t at $t = 0$ yields the subsurface image

$$\begin{aligned} g(x, z) &= \frac{1}{2\pi} \int d\omega \, e^{i\omega t} \, W(\omega, x, z) \mid_{t=0} \\ &= \frac{1}{4\pi^2} \int d\omega \int dk_x \, e^{i2\omega \int_0^z d\zeta \, \frac{\cos\theta(k_x/\omega,\zeta)}{v(\zeta)} + ik_x x} \, F(\omega, k_x). \end{aligned} \tag{5}$$

Equation (5) concisely summarizes the zero-offset phase-shift migration method in isotropic media (Hale, 1992).

Output data after time migration, however, are usually presented as a function of two-way vertical traveltime, τ, rather than depth. Substituting $\tau = 2\int_0^z \frac{d\zeta}{v}$ and $d\tau = 2\frac{dz}{v(\zeta)}$ into equations (4) and (5) yields

$$W(\omega, x, \tau) = \frac{1}{2\pi} \int dk_x \, e^{i\omega \int_0^\tau d\zeta \, \cos\tilde{\theta}(k_x/\omega,\zeta) + ik_x x} \, F(\omega, k_x), \tag{6}$$

and

$$g(x, \tau) = \frac{1}{4\pi^2} \int d\omega \int dk_x \, e^{i\omega \int_0^\tau d\zeta \, \cos\tilde{\theta}(k_x/\omega,\zeta) + ik_x x} \, F(\omega, k_x), \tag{7}$$

where $\tilde{\theta}(\tau) = \theta[\frac{1}{2}\int_0^\tau v(\zeta) d\zeta]$.

Kitchenside (1991) and Gonzalez et.al. (1991) showed the earliest implementations of poststack phase-shift migration in anisotropic media. In VTI media, velocity varies with phase angle, $\tilde{\theta}$, and, therefore,

$$\sin\tilde{\theta}(p_x, \tau) = V(\tilde{\theta}, \tau) p_x,$$

where V is the phase velocity, and

$$\tau = 2\int_0^z \frac{d\zeta}{V(0, \zeta)},$$

where $V(0, \zeta)$ is the vertical P-wave velocity ($=V_{P0}$). Setting $p_\tau = \frac{\cos\tilde{\theta}(k_x/\omega,\zeta)V(0,\zeta)}{V(\tilde{\theta},\zeta)}$ (The velocity-normalized vertical component of slowness), equation (6) becomes

$$W(\omega, x, \tau) = \frac{1}{2\pi} \int dk_x \, e^{i\omega \int_0^\tau d\zeta \, p_\tau(k_x,\omega,\zeta) + ik_x x} \, F(\omega, k_x), \tag{8}$$

and equation (5) becomes

$$g(x, \tau) = \frac{1}{4\pi^2} \int d\omega \int dk_x \, e^{i\omega \int_0^\tau d\zeta \, p_\tau(k_x,\omega,\zeta) + ik_x x} \, F(\omega, k_x), \tag{9}$$

which concisely summarizes the zero-offset phase-shift migration method in VTI media.

Prestack phase-shift migration

To perform the phase-shift migration in the prestack domain, the zero-offset dispersion relation must be replaced by the double-square-root (DSR) equation. An additional Fourier transform over offset is also needed.

Constant velocity prestack migration, with output provided in two-way vertical time, in offset-midpoint coordinates (Yilmaz, 1979) in given by:

$$g(t=0,k_x,h=0,\tau)=\int d\omega \int dk_h\; e^{i\omega \tilde{p}_\tau(p_x,p_h)\tau} F(\omega,k_x,k_h,\tau=0), \tag{10}$$

where $F(\omega,k_x,k_h,\tau=0)$ is the 3-D Fourier transform of the field $f(t,y,h,\tau=0)$ recorded at the surface using:

$$F(\omega,k_x,k_h,\tau=0)=\int dt\; e^{-i\omega t}\int dy e^{i\omega k_x x}\int dh e^{i\omega k_h h} f(t,x,h,\tau=0),$$

and $k_x = 2\omega p_x$, $k_h = 2\omega p_h$, and $k_z = 2\frac{\omega}{v}p_\tau$. In this paper, I will freely alternate between the half offset, h, and the full offset, X, in representing the offset axis, where $X = 2h$. The phase factor $\tilde{p}_\tau(p_x,p_h)$, for isotropic media, is defined in the dispersion relation as

$$\tilde{p}_\tau(p_x,p_h) \equiv \frac{1}{2}(\left[1-v^2(p_x+p_h)^2\right]^{\frac{1}{2}}+\left[1-v^2(p_x-p_h)^2\right]^{\frac{1}{2}}), \tag{11}$$

which is a normalized version of the double-square-root (DSR) equation. The two integrals in ω and k_h in equation (10) represent the imaging condition for zero-offset and zero time ($h=0, t=0$).

Equation (10) with the proper values of p_h and p_x to avoid imaginary values of $\tilde{p}_\tau$ (Popovici, 1993) can be used to do prestack migration. To obtain real values of p_τ that satisfy the downward continuation ordinary differential equation

$$\frac{\partial^2 W}{\partial \tau^2} = -\omega^2 \tilde{p}_\tau^2 W, \tag{12}$$

p_x and p_h must satisfy:

$$\begin{cases} \frac{1}{v} & \geq & \mid p_x + p_h \mid \\ \frac{1}{v} & \geq & \mid p_x - p_h \mid . \end{cases}$$

Both conditions are satisfied by insuring that

$$\mid p_x \mid + \mid p_h \mid \;\; \leq \;\; \frac{1}{v}. \tag{13}$$

The DSR migration can be put in a form to allow for separate migration of each constant-offset section (Popovici, 1993). For migration of a separate offset section, $F(\omega,k_x,h_0,\tau=0)$, equation (10) becomes

$$g(t=0,k_x,h=0,\tau)=\int d\omega \int dk_h\; e^{i\omega[\tilde{p}_\tau(p_x,p_h)\tau+2p_h h_0]} F(\omega,k_x,h_0,\tau=0), \tag{14}$$

where h_0 is the half-offset of that section.

The k_h integral can be evaluated using the stationary phase method. As shown in Appendix A, the stationary point for isotropic homogeneous media is obtained by finding the maximum (with respect to p_h) of the following equation:

$$T(p_h) = 0.5\tau \left[\sqrt{1.0 - (p_x + p_h)^2 v^2} + \sqrt{1.0 - (p_x - p_h)^2 v^2} \right] + 2p_h h. \tag{15}$$

Figure 1 shows T, with p_τ given by equation (17), as a function of p_h for p_x=0 (a horizontal reflector) and for p_x=0.2 (a dipping reflector). To insure that p_τ remains real, p_h in Figure 1 ranges between 0 and $\frac{1}{v} - p_x$. Clearly, T in Figure 1 is multivalued; The first branch, corresponding to lower T values, represents the case in which rays from both the source and receiver have angles less than 90 degrees with the vertical (at the reflection point). The second branch corresponds to rays from either the source or receiver being overturned at the reflection point. Although the second branch is not applicable to homogeneous media (rays have always a 90-degree or less angle with the vertical), it has important implications for overturned rays in $v(z)$ media. For large offsets and steep reflectors in a $v(z)$ medium, the maximum of T (stationary point solution) usually exists in the second branch (higher T values).

Notice the relatively small curvature that T experiences near its maximum (the solution of the stationary phase problem). The curvature is even smaller for the dipping reflector example. This is a key to obtaining good analytical approximations in solving for p_h. The insensitivity of T to p_h around the solution implies that even an imperfect p_h can result in a good estimate of T. When all is said and done, it is the accuracy of T, which describes the phase shift, that matters the most.

For VTI media, T is slightly more complicated than its isotropic counterpart, and is given by

$$T(p_h) = 0.5\tau \left[\sqrt{1 - \frac{(p_x + p_h)^2 v^2}{1 - 2\eta v^2 (p_x + p_h)^2}} + \sqrt{1 - \frac{(p_x - p_h)^2 v^2}{1 - 2\eta v^2 (p_x - p_h)^2}} \right] + 2p_h h \tag{16}$$

Appendix B. Figure 2 shows T for a VTI medium with v=2 km/s and η=0.2, again for a horizontal reflector (p_x=0) and a dipping one (p_x=0.2). Now, p_h ranges between 0 and $\frac{1}{v\sqrt{1+2\eta}} - p_x$, because $pv\sqrt{1+2\eta}$, where p is the ray parameter and must be smaller or equal 1 to avoid evanescent waves. The conclusion regarding the curvature and its implications, described in the isotropic case, holds here as well.

SEPARATE-OFFSET PRESTACK MIGRATION

To implement prestack phase-shift migration, we need to evaluate the phase (or T) for which the data will be shifted. Unlike zero-offset migration, where p_h=0, and therefore the phase can be determined directly, in separate-offset prestack migration

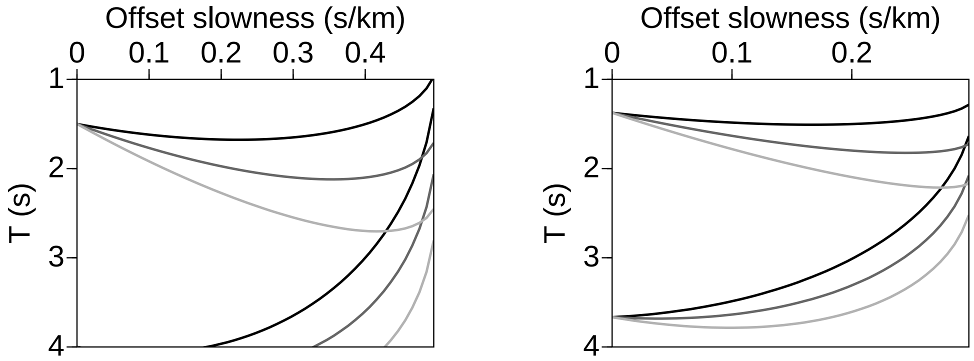

Figure 1: Left: the phase factor, T, as a function p_h for a horizontal reflector (p_x=0). Right: T as a function p_h for a dipping reflector (p_x=0.2). The medium is isotropic and homogeneous with v=2 km/s. The black curve corresponds to an offset-to-vertical-time ratio ($\frac{X}{\tau}$) of 1.0 km/s, the dark-gray curve corresponds to $\frac{X}{\tau}$=2.0 km/s, and the light gray curve corresponds to $\frac{X}{\tau}$=3.0 km/s. tariq1-tploteta0 [NR]

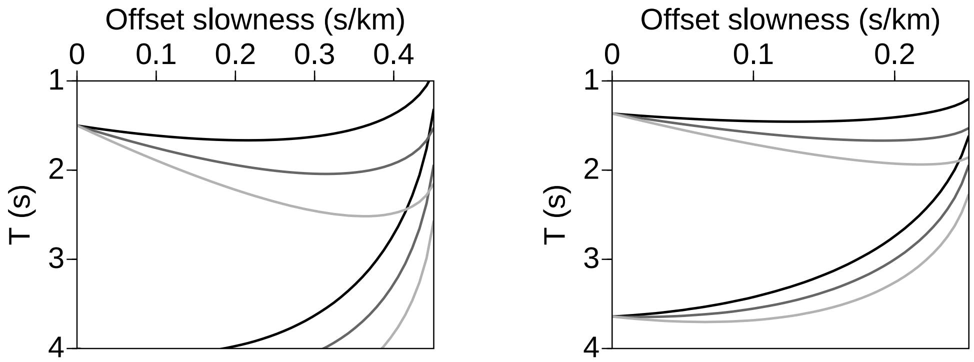

Figure 2: Same as in Figure 1, but for a VTI medium with η=0.2. tariq1-tploteta2 [NR]

we must first obtain p_h and then use it to evaluate the phase. The value of p_h can be determined numerically using any number of existing numerical methods (some based on evaluating derivatives), or through using analytical approximations. The efficiency in the numerical implementations is achieved by setting up numerous precomputed traveltime tables at different stages of the migration. These tables are necessary to avoid redundancy in calculations. The analytical solutions, on the other hand, are restricted, at this point, to homogeneous isotropic and VTI media. [4]

Numerical solutions of p_h

To implement prestack phase-shift migration efficiently in $v(z)$ media, we need to construct a table of $\tau(p_x, t)$ using ray tracing, where τ is the vertical two-way traveltime and t is the two-way zero-offset traveltime. Due to the lateral homogeneity assumption, this table is constructed once and is applicable everywhere. The stationary point is evaluated by finding

$$\max\{T\}, \tag{17}$$

where

$$T = 0.5[\tau(p_x + p_h, t) + \tau(p_x - p_h, t)] + 2p_h h, \tag{18}$$

and

$$\tau(p_x, t) = \int_0^t p_\tau(p_x, \zeta) d\zeta,$$

where p_τ is the zero-offset normalized dispersion factor, shown just above equation (8).

To find the maximum of equation (18), I use a method described by Buchanan and Turner (1992). This is a robust algorithm used to find a maximum or minimum of a function numerically without the need to resort to evaluating derivatives (similar in principal to the bisection method used to evaluate roots of functions). Other methods, based on the finding the roots of the derivative of equation (18) with respect to p_h, will most likely fail due to the sensitivity of these derivatives to typical numerical errors associated with ray tracing. Another table, $\tilde{T}(p_x, t)$, consisting of T for the solutions of equation (17) for given p_x, time, and offset is, therefore, constructed. Again, such a table is applicable everywhere in the medium due to the lateral homogeneity assumption considered here. The cost of a prestack migration of any offset is about 10% higher than that for a zero-offset algorithm, where p_h=0 is known, and thus we do not need to evaluate it. This relatively small additional cost reduces even further when large data sets are migrated and the cost of precomputing the traveltime tables become insignificant.

[4] Implications, where $v(z)$ migration is a necessity, is beyond the scope of this paper and it will be discussed in a follow up paper.

Analytical approximations of p_h

Although the numerical solutions are sufficient and efficient enough to perform prestack migration, analytical solutions are important for obtaining insights into the problem. Analytical solutions are also important for inversion purposes where we need to calculate the solution and its derivatives for different medium parameters in an iterative fashion.

For homogeneous isotropic media, the stationary point is given by

$$p_h = \frac{\frac{X}{\tau}}{v\sqrt{(\frac{X}{\tau})^2 + v^2}}(1 - p_x^2 v^2)^{3/2}[a(p_{hs})p_x + 1] \tag{19}$$

(Appendix B), where

$$a = \frac{1}{p_{h0}(1 - p_x^2 v^2)^{3/2}} - \frac{1}{p_{hs}}.$$

and p_{h0} and p_{hs} are given in the Appendix. This equation is obtained by fitting p_h to it's exact solution at three different values of p_x, and therefore, I will refer to it as the 3-point solution. For $p_x = 0$, although not directly obvious, equation (19) reduces to

$$p_h = \frac{\frac{X}{\tau}}{v\sqrt{(\frac{X}{\tau})^2 + v^2}},$$

which corresponds to the exact stationary point solution for horizontal reflectors. As demonstrated in Appendix B, this equation can be extracted directly from the hyperbolic moveout relation for a homogeneous isotropic medium. The other two terms in equation (19), the ones in circular and square brackets, insure that we obtain the exact solution of the stationary point at $p_x = p_h$, and $p_x = \frac{1}{v}$, respectively.

The 2-point solution, shown in Appendix B, is the same as equation (19) without the term in square brackets. As a result, this equation fits the exact solution at $p_x = 0$ and $p_x = \frac{1}{v}$, and, therefore, I will refer to it as the 2-point solution. The low curvature of T around its maximum (see Figure 1) makes any error attributed to equation (19) or to the 2-point solution to be insignificant, even for large offsets.

The stationary point solutions for homogeneous VTI media are much more complicated, as shown in Appendix B, than their isotropic counterparts. Nevertheless, they have the same form (2- and 3-point fitting solutions) as that for isotropic media. The solutions for $p_x = 0$ and $p_x = p_h$, however, are no longer exact because we dropped some terms (related to strong anisotropy and large offsets) in their derivation. Nevertheless, the approximations, as shown in Appendix B and in the following subsection, are relatively accurate. In fact, using the perturbation theory along with Shanks transforms, one can obtain even better approximations of p_h (see Appendix C).

Phase calculations

Once the offset ray parameter (p_h), or an approximation of it, is determined, it is then used, along with equation (18), to calculate traveltime (phase shifts). What makes zero-offset migration so trivial is that p_h is known in advance ($p_h = 0$), and therefore, traveltime calculation can be done directly. For prestack migration, we must first estimate p_h then precede with traveltime calculations. Although p_h above can be evaluated using analytical approximations, the phase will always be evaluated by inserting the value of p_h into the exact DSR equation [i.e., equation (18)].

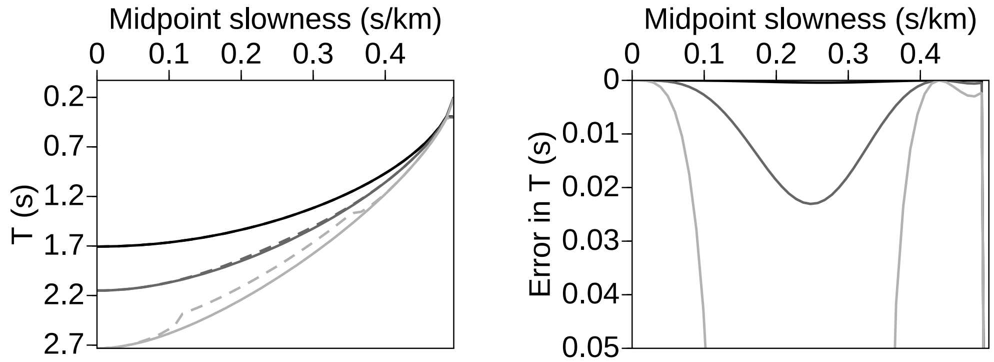

Figure 3: Left: the phase correction, T, as a function p_x using p_h calculated numerically (solid curve), and p_h calculated using the 2-point solution (dashed curve). Right: The absolute difference between each of the two curves (numerical and analytical) on the left. The medium is homogeneous and isotropic with v=2.0 km/s. The black curve corresponds to an offset-to-vertical-time ratio ($\frac{X}{\tau}$) of 1.0 km/s, the dark-gray curve corresponds to $\frac{X}{\tau}$=2.0 km/s, and the light-gray curve corresponds to $\frac{X}{\tau}$=3.0 km/s. tariq1-t2eta0m [NR]

Figures 3 through 7 compares T [where ωT constitutes the phase of the integral of equation (14)] evaluated using numerical solutions of p_h with those obtained via analytical approximations using either the 2-point, the 3-point, or perturbation-theory solutions of p_h.

For isotropic homogeneous media, T calculated using the 3-point solution of p_h better approximates the T derived from the numerical solutions than that given by the 2-point solution (compare Figures 3 and 4). As expected, errors will increase, for all cases, with increasing offsets. However, because $\frac{X}{\tau}$=3 km/s [offset-to-depth ratio (X/D) of 3] is rarely encountered in practice, and usually falls far within the typical mute zone, these approximations yield fairly accurate phase shifts even for practical large offsets. The irregularity in the T curve in Figure 3, for p_h calculated using the 2-point solution and $\frac{X}{\tau} = 3$ km/s, is a result of enforcing the condition that $p_x + p_h \leq \frac{1}{v}$, which is necessary to avoid imaginary values in the DSR equation.

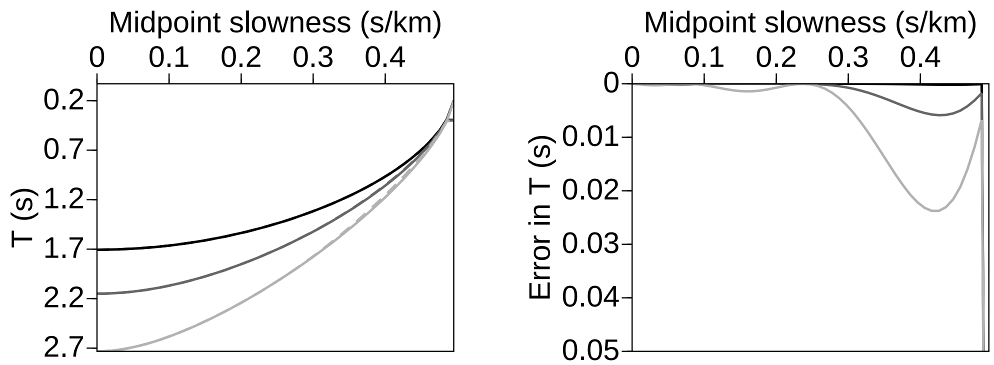

Figure 4: Same as in Figure 3, but now we are comparing the numerical solution with that obtained for p_h calculated using the analytical 3-point fitting equation. tariq1-t3eta0m [NR]

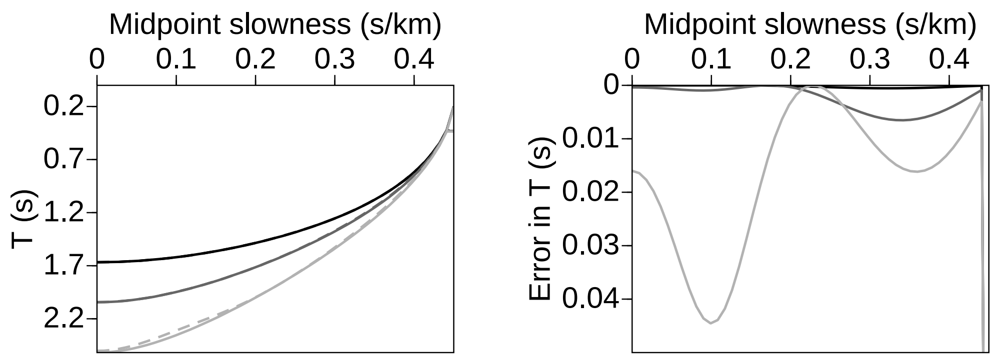

Figure 5: Same as in Figure 3, but the medium now is VTI with η=0.2. tariq1-t2eta2m [NR]

In VTI media, only for $\frac{X}{\tau}$=1 km/s, the T derived using the 3-point solution better approximates the numerical solution than T derived using the 2-point solution (compare Figures 5 and 6). The degradation of the 3-point solution at large offsets can be attributed to the failure of the $p_x = p_h$ fitting approximation to improve the results for such offsets. For large offsets we are approaching the validity limit of the 3-point solution. A strict condition is enforced upon the p_h derived from setting $p_x = p_h$ (see Appendix B). Although we have obviously met this condition (or otherwise we would have gotten imaginary solutions), coming close to the limit has clearly negatively effected the solution. Between the 2-point fitting solution and the 3-point one, one might want to implement a weight factor that favors the 3-point solution at near offset and the 2-point solution at far offset.

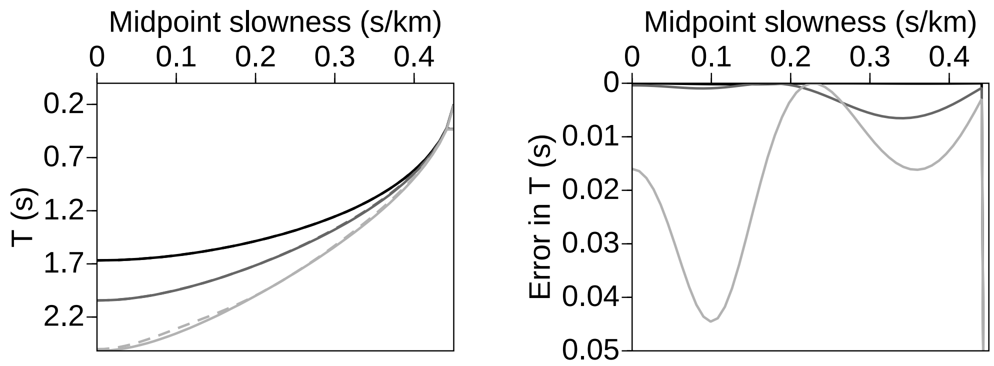

Figure 6: Same as in Figure 4, but the medium now is VTI with η=0.2. tariq1-t3eta2m [NR]

Using perturbation theory and Shanks transform (Appendix C; Bender and Orszag, 1978), we can obtain even better 3-point fitting estimations of the stationary point solution for VTI media, much better than the previous 2- or 3-point solutions. In fact, Figure 7 consists of two sets of curves (corresponding to the numerical solutions and analytical ones derived using Shanks transforms) that practically overlap for all p_x. The difference, given by the right curve, shows that the errors are lower than any previously obtained solutions.

What's especially remarkable here is the high level of accuracy achieved with imaging horizontal reflectors despite the approximations used in developing p_h for such a reflector dip; the error is almost zero for even the $\frac{X}{\tau}$=3 km/s (X/D=3) example (see Figure 7). The accuracy achieved here far exceeds the ones obtained via Taylor series expansions (or even modifications of it) of traveltime around X=0 (Alkhalifah, 1997b). This analytical result has significant implications for non-hyperbolic moveout inversion in VTI media.

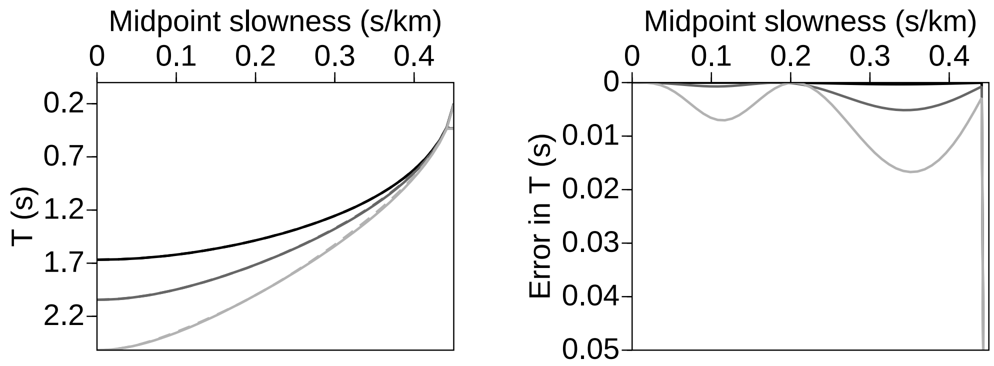

Figure 7: Same as in Figure 4, but the medium now is VTI with η=0.2. Here I am using the perturbation theory and Shank transform. tariq1-t3sheta2m [NR]

SYNTHETIC DATA EXAMPLES

In the following synthetic examples, I will compare migration implemented using analytical solutions of p_h with that using numerical solutions. Unless otherwise stated, all the examples are for anisotropic media (η >0), hinging on the fact that what works for anisotropic media should work for a subset of it, namely isotropic media. [5]

Figure 8 shows impulse responses of an impulse input at 1.8 s into the prestack time migration algorithm, for a VTI medium with v=2.0 km/s and η=0.3. The offset considered here is 2.0 km. The first response was obtained using the prestack phase-shift migration with analytically derived values of p_h (using the 3-point Shanks-transform solution). The second response is also obtained using prestack phase-shift migration but now with numerically derived values of p_h. The final response resulted from inputing the impulse into an NMO correction algorithm, followed by the VTI dip-moveout (DMO) algorithm of Alkhalifah (1996), and then a VTI post-stack phase-shift migration. The DMO is based on the dip-decomposition method of Jakubowicz (1990). The responses are practically identical and therefore the output of applying these algorithms on real data should be similar. The advantage of the phase-shift method (the numerical version) is its ability to handle complex velocity functions. Figure 9 shows the difference between the numerically derived p_h prestack migration response with the analytically derived one. The largest difference, as can be predicted from Figure 7, occurs at steep dips. Although kinematically the prestack and poststack approaches are similar, the DMO approach suffers from aliasing associated with improper sampling of the dip component, which appears when media with sharp velocity variations are treated. Such aliasing can somewhat be avoided by reducing

[5]Also, I am convinced that media of an isotropic nature does not exist in the subsurface, it only exits in synthetic data like the Marmousi model.

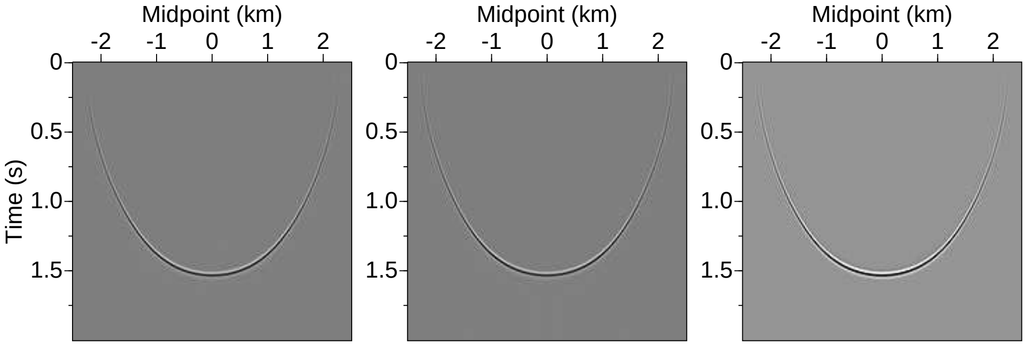

Figure 8: Prestack time-migration impulse responses of an impulse at 1.8 s for a VTI medium with v=2.0 km/s and η=0.3. Left: the response was generated using the prestack phase-shift method with p_h estimated analytically (using the Shanks transform solution). Center: the response was generated also using the phase-shift method with p_h calculated numerically. Right: the response was generated by applying NMO, VTI DMO (Alkhalifah, 1996), and zero-offset phase-shift migration to the impulse. tariq1-imp2 [NR]

the dip-decomposition sampling; however, this comes at larger cost of implementing the DMO. On the other hand, the response of the phase-shift migration does not show any of such aliasing artifacts, and the operator is thus cleaner.

Figure 10 shows a model consisting of horizontal reflectors and dipping ones with dip angles ranging from 30 to 90 degrees at 15-degree intervals. The 90-degree reflector is not imaged in a homogeneous medium due to the limited aperture. Even the 75-degree one suffers from such a limit in the aperture. Figure 11 shows synthetic common-offset sections generated for a VTI medium with v=2.5 km/s and η=0.3. The left section corresponds to an offset of 2 km, the right one to an offset of 4 km. Figure 12 shows the result of prestack migration using the numerically derived p_h. For all practical purposes, the migrated images are identical and accurate.

Figure 13 shows the migration of Figure 11 using analytically derived values of p_h. Specifically, I am using the Shanks-transform 3-point solution of p_h because the medium is strongly anisotropic. The imaged section resembles the one obtained using numerical solutions of p_h. The artifacts notable in the 4 km offset migrated section in Figure 13 are well within the typical mute zone, and they result from the limitations of the approximations to handle such large offset-to-depth ratios (> 3) and such a strong anisotropy (η=0.3). For 4 km offset and $v = 2.5$ km/s velocity, a typical mute time (a time where all samples prior to it are set to zero) is about 1.5 s.

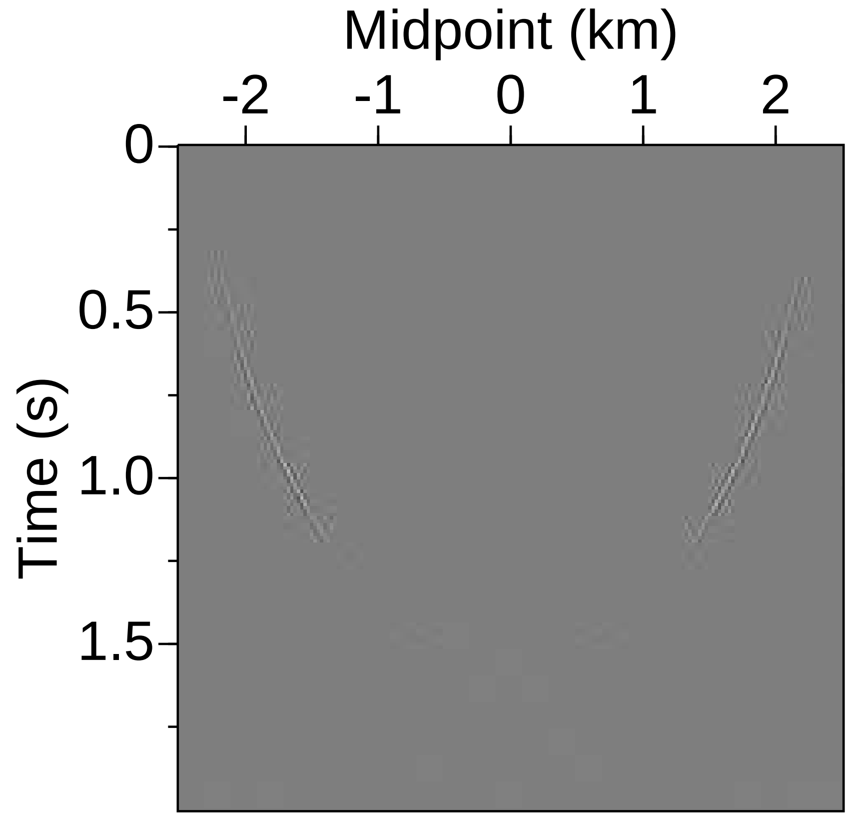

Figure 9: The difference between the prestack phase-shift migration responses shown in Figure 8 (the two on the left), plotted at the same amplitude scale as those in Figure 8. tariq1-impdiff [NR]

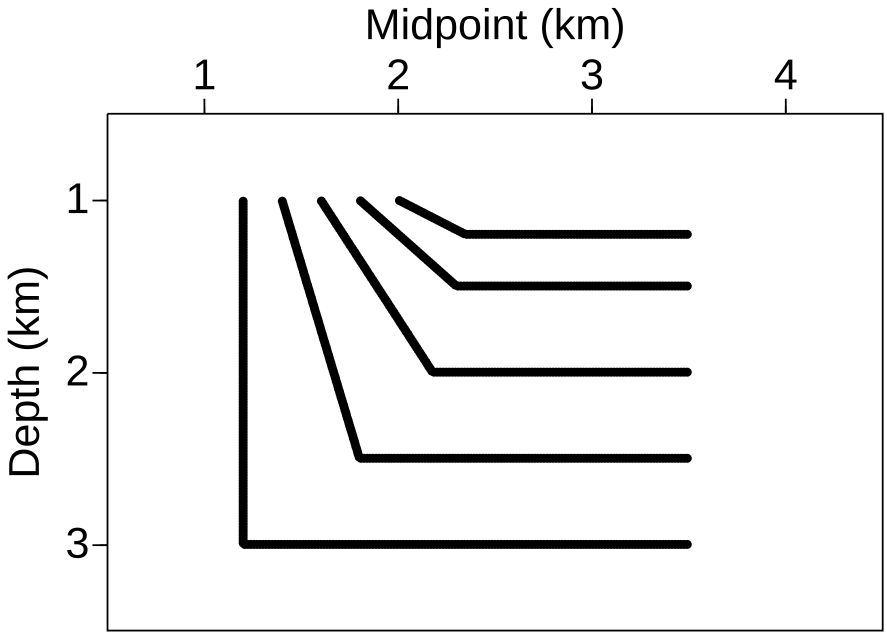

Figure 10: Reflector model containing reflectors dipping at 0, 30, 45, 60, 75, and 90 degrees. tariq1-model [NR]

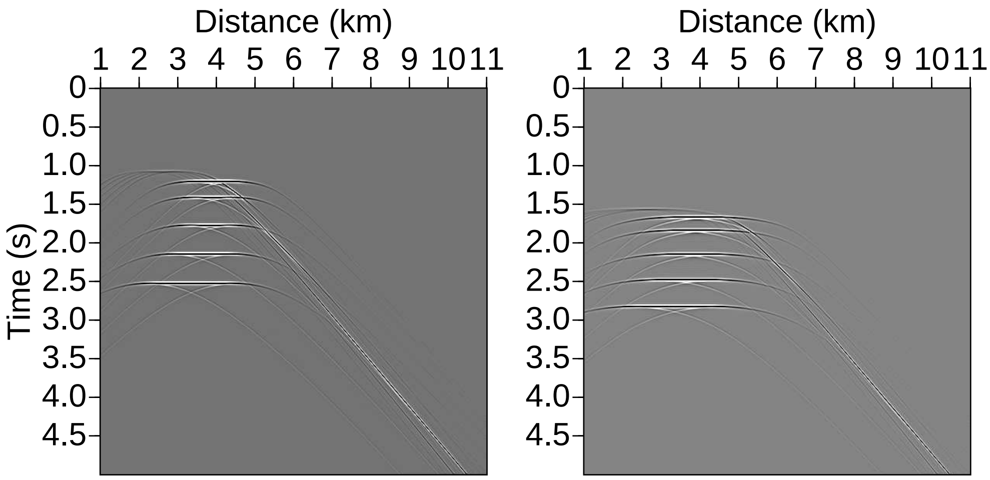

Figure 11: Common-offset synthetic data from the reflector model in Figure 10 for an offset of 2 km (left), and an offset of 4 km (right). The medium is VTI with velocity of 2.5 km/s and η=0.3. tariq1-synti3 [NR]

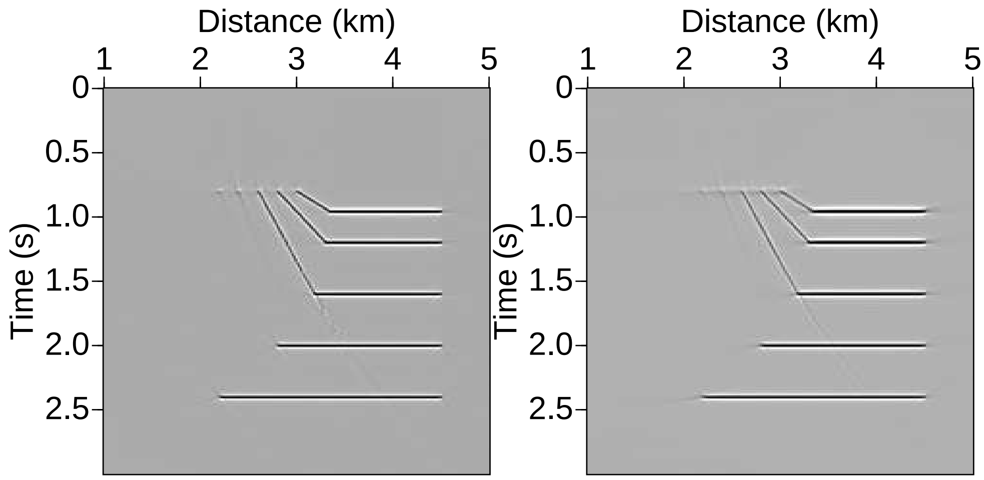

Figure 12: Prestack phase-shift migrated section, using numerically derived p_h values, of the data in Figure 11 for an offset of 2 km (left), and an offset of 4 km (right). The mute level was somewhat relaxed to allow for maximum data exposure. Major portions of the right section would have not survived typical mute zones. tariq1-migti3 [NR]

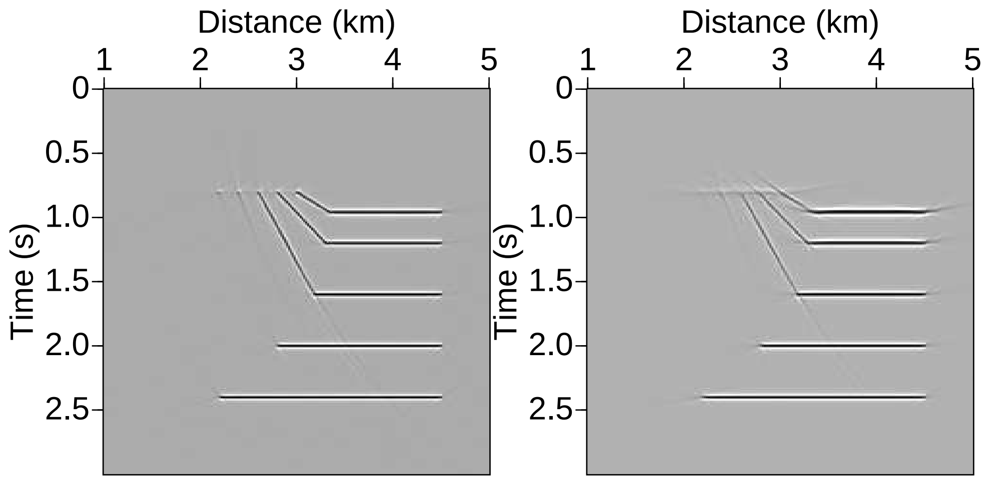

Figure 13: Prestack phase-shift migrated section using analytically derived p_h values of the data in Figure 11 for an offset of 2 km (left), and an offset of 4 km (right). tariq1-miganti3 [NR]

FIELD DATA EXAMPLES

Alkhalifah (1997a) showed images of the subsurface extracted by processing data from offshore Angola (Africa) based on a VTI medium assumption. He used a sequence of NMO, VTI DMO, and VTI zero-offset time migration to process the data. Figure 14 shows the inverted interval velocity and η curves used in Alkhalifah's processing. The large η value prior to 2.5 s correspond to Tertiary shales, the main source of anisotropy in the subsurface (Banik, 1984; Sayer, 1995), as well as in this data.

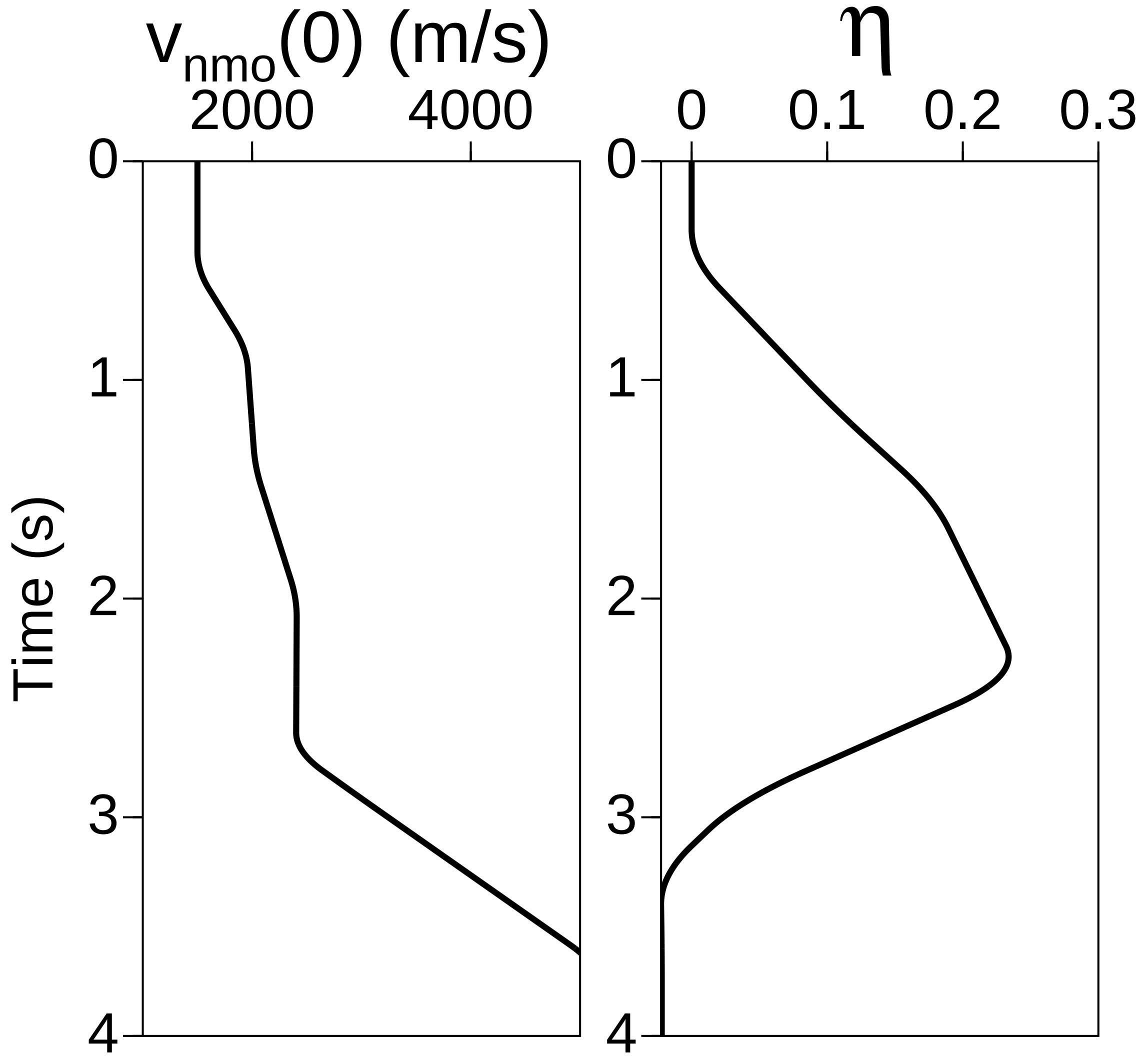

Figure 14: Estimated interval values of v and η as a function of vertical time. tariq1-etavpara2 [NR]

Here, I will apply prestack time migration to this data using the same inverted parameters in Figure 14. The prestack migration is followed by an inverse NMO with a single velocity, velocity analysis, and then an NMO with velocity extracted from the velocity analysis that may vary laterally, vertically, or both. The result of this new combination of processes resembles what I obtained in an earlier paper (Alkhalifah, 1997a), with improvements over the isotropic result very much intact (see Figure 15). Both the faults under CMP locations 400 and 900, between 2 and 2.5 s, which were not manifest in Alkhalifah's isotropic result, showed clearly here.

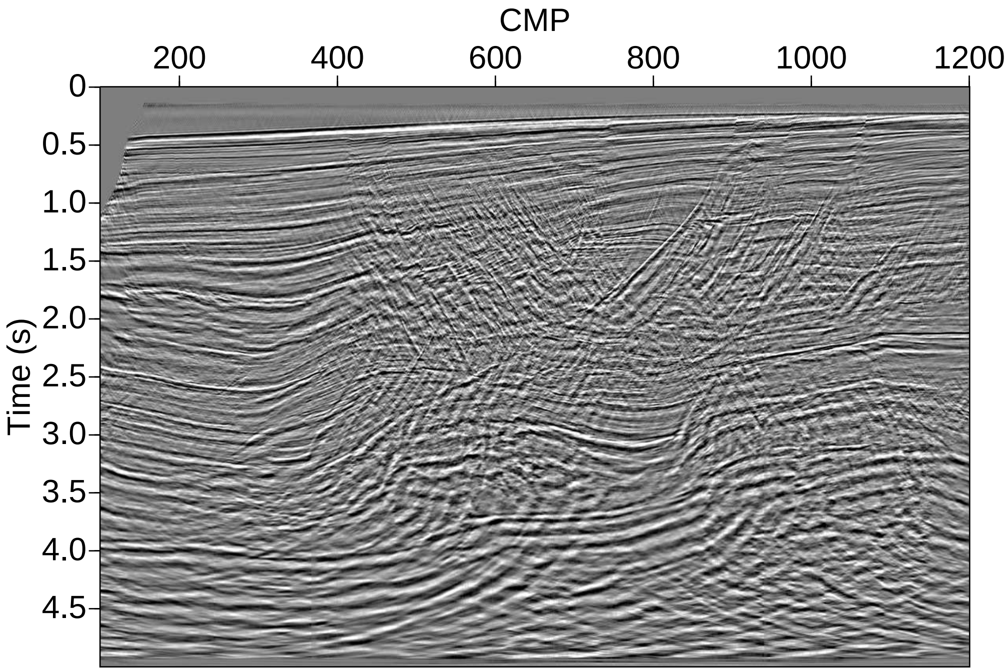

Figure 15: A stacked section of prestack phase-shift migrated data from offshore Angola (Alkhalifah, 1997a) using the parameters in Figure 14. tariq1-migprchev [NR]

Figure 16 shows the result of using the interval NMO velocities in Figure 14 in an isotropic prestack phase-shift migration. The run time for the two migrations (the isotropic and anisotropic one) is practically the same. Yet the anisotropic result is far superior to the isotropic one, especially in focusing the dipping faults. Alkhalifah (1997) arrived at this same conclusion using the poststack processing sequence.

The overall cost, however, of the DMO-based processing is slightly lower than that of prestack phase-shift migration. However, if sharper velocity models are used, the cost of the phase-shift prestack approach will be considerably lower if comparable quality results is the goal. For DMO, increased dip sampling is needed to handle sharper velocity models, and such an increase in dip sampling will influence the speed of the migration negatively.

There are two major numerical differences between the poststack approach which

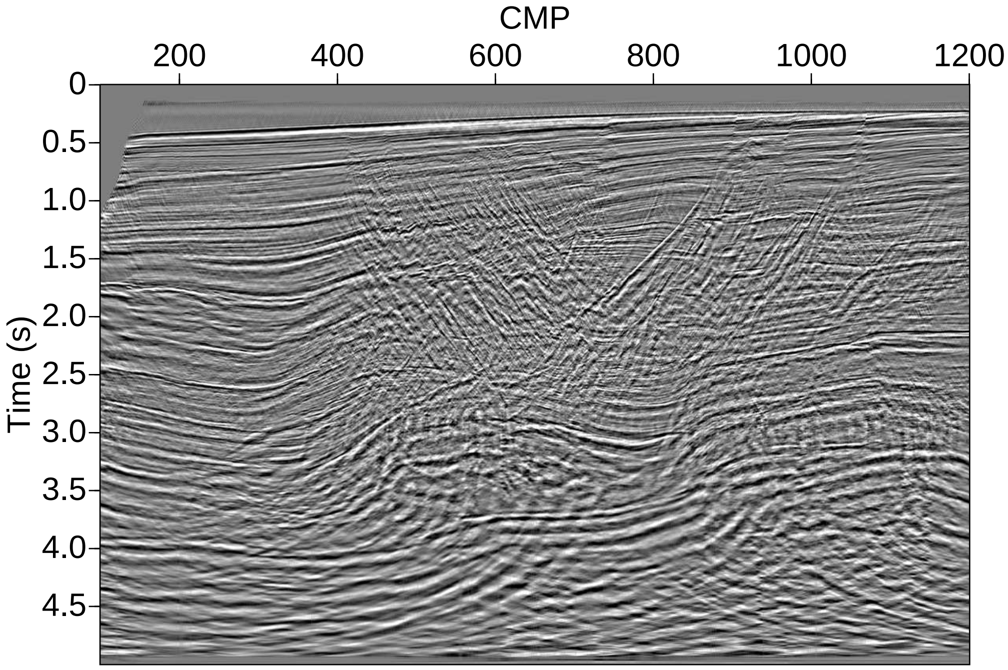

Figure 16: A stacked section of prestack isotropic phase-shift migrated data from offshore Angola (Alkhalifah, 1997a) using only the interval NMO velocities shown in Figure 14. tariq1-migprchevis [NR]

features the dip-decomposition DMO (Alkhalifah, 1996) and the prestack approach described here. First, in the prestack phase-shift method the corrections (NMO, DMO, and zero-offset migration) are all applied to the data in the Fourier domain, where the slopes of the reflection are not yet zero-offset. Such an implementation requires, as we have seen earlier, solving for one unknown parameter (p_h) in order to apply the phase shift in a $v(z)$ model. In contrast, the dip-decomposition DMO requires solving for four unknowns (Artley and Hale, 1994) to handle (within the limit of ray theory) a $v(z)$ model exactly. The large number of unknowns in the DMO approach introduces instability problems in its implementation, especially in handling a complex $v(z)$ model. Working with plane waves, as is the case in the phase-shift method, typically yields much simpler equations than working with point-source waves.

A second difference corresponds to the dip-decomposition approach in which, unless the dip sampling is fine enough, artifacts can occur in the DMO result. Again, this is a problem when sharper velocity models are considered.

CONCLUSION

Unlike zero-offset phase-shift migration, the prestack version, obtained by evaluating the offset-wavenumber integral with the stationary phase method requires solving for the stationary point of the horizontal component of offset slowness (p_h) prior to applying the phase shift. Exact analytical solutions of p_h are hard to obtain, especially for anisotropic media. Numerical solutions of p_h, however, are efficiently obtainable through the use of numerous precomputed tables at different stages of the migration. Given that the phase of the k_x integrand is rather insensitive to p_h around its maximum (around the stationary point solution), p_h can also be estimated using analytical approximations. These analytical equations are obtained by fitting them to the exact solution at different slopes. Errors on the order of 1% in p_h result in less than 0.1% error in the phase because of its relatively low sensitivity to p_h.

For anisotropic media, the analytical solutions include additional approximations based on weak anisotropy. The resultant equations, nevertheless, produce accurate migration signatures for relatively strong anisotropy (i.e., $\eta = 0.4$) and even for large offsets (i.e., offset-to-depth ratios larger than 2). The accuracy of the anisotropic result at zero reflector dip is particularly amazing. Analytically, the accuracy far exceeds anything previously derived using Taylor series expansions (Tsvankin and Thomsen, 1994, Alkhalifah, 1997b).

The numerical implementation of the proposed prestack migration is fast. The cost of prestack migration of a single common-offset section is about 10% higher than the cost of zero-offset migration of the same size section. The additional cost (spent calculating p_h) is reduced even further (percentage wise) when migrating large volumes of data, where the cost of this overhead becomes more and more insignificant.

ACKNOWLEDGEMENT

I thank Chevron Overseas Petroleum Company, specifically to John Toldi, for providing the data.

REFERENCES

Alkhalifah, T., 1996, Transformation to zero offset in transversely isotropic media: Geophysics, **61**, 947-963.

Alkhalifah, T., 1997a, Seismic Data Processing in vertically inhomogeneous TI media: Geophysics, **62**, 662-675.

Alkhalifah, T., 1997b, Velocity analysis using non-hyperbolic moveout in transversely isotropic media: Geophysics, in press.

Alkhalifah, T., 1997c, Acoustic approximations for processing in transversely isotropic media: Geophysics, submitted.

Alkhalifah, T., and Tsvankin, I., 1995, Velocity analysis for transversely isotropic media: Geophysics, **60**, 1550-1566.

Banik, N. C., 1984, Velocity anisotropy of shales and depth estimation in the North Sea basin: Geophysics, **49**, 1411–1419.

Bender, C. M., and Orszag, S. A., 1978, Advanced mathematical methods for scientists and engineers, McGraw-Hill, Inc.

Gazdag, J., 1978, Wave equation migration with the phase-shift method: Geophysics, **43**, 1342–1351.

Gazdag, J., and Sguazzero, P., 1984, Migration of seismic data by phase shift plus interpolation: Geophysics, **49**, 124–131.

Gonzalez, A., Lynn, W., and Robinson, W., 1991, Prestack frequency-wavenumber (f-k) migration in a transversely isotropic medium: Presented at the 61st Ann. Internat. Mtg. Soc. Expl. Geophys., Expanded Abstracts, 1155–1157.

Hale, D., 1992, Migration by the Kirchhoff, slant stack, and Gaussian beam methods: Center of Wave Phenomena (CWP), Report **121**, Colorado School of Mines.

Jakubowicz, H., 1990, A simple efficient method of dip-moveout correction: Geophys. Prosp., **38**, 221–245.

Kitchenside, P. W., 1991, Phase shift-based migration for transverse isotropy, 61st Ann. Internat. Mtg., Soc. Expl. Geophys., Expanded Abstracts, 993-996.

Lynn, W., Gonzalez, A., and MacKay, S., 1991, Where are the fault-plane reflections?, 61st Ann. Internat. Mtg., Soc. Expl. Geophys., Expanded Abstracts, 1151–1154.

Popovici, M., 1993, Prestack phase-shift migration for separate offsets: SEP-**79**, 115-127.

Popovici, M., 1995, Migration to zero offset, Ph.D. thesis, Stanford University.

Press, W.H., Teukolsky, S.A. Vetterling, W.T., and Flannery, B.P., 1992, Numerical recipes in C, the art of scientific computing, 2nd Edition, Cambridge University Press, New York.

Sayers, C.M., 1994, The elastic anisotropy of shales: J. Geophys. Res., **99**, No. B1, 767-774.

Stoffa, P. L.,and Fokkema, J. T., de Luna Freire, R. M., Kessinger, W. P., 1990, Split-step Fourier migration: Geophysics, **55**, 410-421.

Stolt, R.H., 1978, Migration by Fourier tranform: Geophysics, **43**, 23-48.

Thomsen, L., 1986, Weak elastic anisotropy: Geophysics, **51**, 1954–1966.

Tsvankin, I., and Thomsen, L., 1994, Non-hyperbolic reflection moveout in anisotropic media: Geophysics, **59**, 1290-1304.

Uzcategui, O., 1995, 2-D depth migration in transversely isotropic media using explicit operators: Geophysics, **60**, 1819-1829. Geophysics, **20**, 780-806.

Yilmaz, O.,1979, Prestack partial migration: Ph.D. thesis, Stanford University.

Zauderer, E., 1989, Partial Differential Equations of Applied Mathematics: Wiley-Interscience.

APPENDIX A

STATIONARY PHASE APPROXIMATION

Downward continuation using the DSR equation for a separate constant-offset section requires the computation of the integral in equation (14). This can be done for a single offset by finding a stationary phase approximation to the integral

$$I = \int dk_h \; e^{i\omega[p_\tau(p_x,p_h)\tau + 2p_h h]}. \tag{A-1}$$

Integrals of the form

$$I(k) = \int_{-\infty}^{\infty} e^{ik\phi(t)} f(t)\; dt$$

are approximated asymptotically (Zauderer, 1989) when $k \to \infty$ by

$$I(k) \approx e^{ik\phi(t_0)} f(t_0) e^{\mathrm{sign}(\phi''(t_0))\frac{i\pi}{4}} \left[\frac{2\pi}{k \mid \phi''(t_0) \mid}\right]^{\frac{1}{2}} \tag{A-2}$$

where t_0 is the "stationary point" in which the derivative of the phase is zero. The approximation described here assumes the second derivative is non-zero, which is the case here, as Popovici (1993) has demonstrated.

The phase of the exponential for homogeneous isotropic media is

$$\phi(p_h) = 0.5\tau \left[\, \sqrt{1.0 - v^2(p_x+p_h)^2} + \sqrt{1.0 - v^2(p_x-p_h)^2}\, \right] + 2p_h h. \tag{A-3}$$

In order to evaluate the stationary point, we need to find the roots of the equation

$$\phi'(p_h) = X + 0.5\tau \left[\frac{p_h+p_x}{\sqrt{1.0 - v^2(p_x+p_h)^2}} + \frac{p_h-p_x}{\sqrt{1.0 - v^2(p_x-p_h)^2}}\right]. \tag{A-4}$$

To find the root we need to solve a sixth-order polynomial. Approximate solutions are presented in Appendix B.

The second derivative of the phase is non-zero, because it consists of the sum of four positive terms (Popovici, 1993):

$$\begin{aligned} \phi''(p_h) \;=\; & \frac{0.5}{\sqrt{1.0 - v^2(p_x-p_h)^2}} + \frac{0.5(p_h-p_x)^2}{4[1.0 - v^2(p_x-p_h)^2]^{\frac{3}{2}}} + \\ + \; & \frac{0.5}{\sqrt{1.0 - v^2(p_x+p_h)^2}} + \frac{0.5(p_h+p_x)^2}{4[1.0 - v^2(p_x+p_h)^2]^{\frac{3}{2}}}\,. \end{aligned} \tag{A-5}$$

This ensures that there is no change in curvature, and that the phase always has a maximum or a minimum and, therefore, a stationary point. Indeed, for a fixed pair of values ω, p_x, Figure A-1 shows the phase function for several depth levels.

APPENDIX B

ANALYTICAL APPROXIMATIONS OF THE STATIONARY POINT SOLUTIONS

Although the numerical solutions are sufficient and efficient enough to perform prestack migration, analytical solutions are important for obtaining insights into the problem. Analytical representations are also important for inversion purposes where the solution is calculated multiple times for different medium parameters in an iterative fashion.

Isotropic homogeneous media

In order to evaluate the stationary point (the point in which the phase is minimum or maximum), we need to solve the equation

$$\frac{\partial T(p_x, p_h, v, \frac{X}{\tau})}{\tau \partial p_h} = 0.5\left(\frac{(p_x + p_h)v^2}{\sqrt{1-(p_x+p_h)^2v^2}} - \frac{(p_x - p_h)v^2}{\sqrt{1-(p_x-p_h)^2v^2}}\right) + \frac{X}{\tau} = 0. \quad \text{(B-1)}$$

Equation (B-1) reduces to the condition that the horizontal projection for rays from each of the source and receiver to the specular reflection point (SRP) add up to equal the source-receiver offset, X (Popovici, 1995). Solving equation (B-1) in its full form involves solving a sixth-degree polynomial, which I prefer to avoid doing analytically.

Setting p_x=0 in equation (B-1) yields solutions (stationary points) for reflections from horizontal reflectors, and, therefore, equation (B-1) reduces to

$$\frac{\partial T(p_h, v, \frac{X}{\tau})}{\tau \partial p_h} \Big|_{p_h = p_{h0}} = \frac{p_{h0} v^2}{\sqrt{1 - p_{h0}^2 v^2}} + \frac{X}{\tau} = 0, \quad \text{(B-2)}$$

with a stationary point given by

$$p_{h0} = \frac{\frac{X}{\tau}}{v\sqrt{(\frac{X}{\tau})^2 + v^2}}. \quad \text{(B-3)}$$

In fact, p_{h0} is the exact stationary point solution for horizontal reflections, which can be derived directly from the hyperbolic moveout equation:

$$t^2 = \tau^2 + \frac{X^2}{v^2}.$$

Where $p_h = \frac{\partial t}{\partial X} = \frac{1}{2}\frac{\partial t}{\partial h}$,

$$p_h = \frac{X}{v^2 t} = \frac{X}{v\sqrt{X^2 + \tau^2 v^2}},$$

which is the same as equation (B-3).

Expanding equation (B-1) using Taylor's series around p_h=0, and ignoring terms beyond the linear in p_h, yields

$$\frac{p_h v^2}{(1 - p_x^2 v^2)^{3/2}} + \frac{X}{\tau} = 0,$$

with a stationary point given by

$$p_h = \frac{\frac{X}{\tau}}{v}(1 - p_x^2 v^2)^{3/2}. \qquad \text{(B-4)}$$

Equation (B-4) corresponds to the exact solution for a vertical reflector, where p_h=0 and $p_x = \frac{1}{v}$. It also provides a good approximation away from $p_x = \frac{1}{v}$. Figure B-1 shows a comparison between the exact p_h solution of equation (B-1) (obtained numerically) and that given by equation (B-4) as a function of p_x for three sets of $\frac{X}{\tau}$. The absolute difference between the two solutions is also displayed. As expected, errors increase with offset, and the accuracy of the approximate solution reduces at

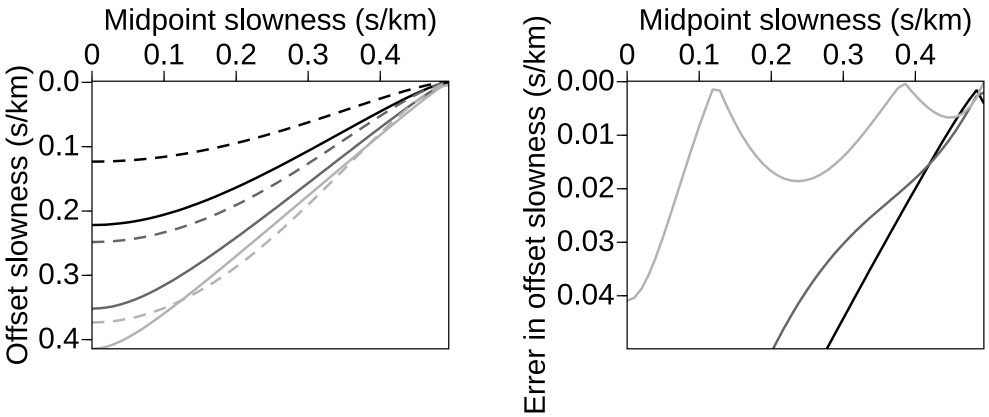

Figure B-1: Left: Values of p_h as a function p_x calculated numerically (solid curves), and calculated analytically (dashed curves)using equation (B-4). Right: The absolute difference between the two curves on the left. The medium is homogeneous and isotropic with v=2.0 km/s. The black curve corresponds to $\frac{X}{\tau}$=1.0 km/s, the dark-gray curve corresponds to $\frac{X}{\tau}$=2.0 km/s, and the light gray curve corresponds to $\frac{X}{\tau}$=3.0 km/s. tariq1-ph1eta0m [NR]

p_x=0. In fact, for p_x=0, p_h in equation (B-4) equals $\frac{\frac{X}{\tau}}{2v}$ which is clearly different from the exact solution given by equation (B-3). Inserting the exact solution, in place of the factor $\frac{\frac{X}{\tau}}{2v}$, in equation (B-4) yields a new approximate solution for p_h given by

$$p_h = \frac{\frac{X}{\tau}}{v\sqrt{(\frac{X}{\tau})^2 + v^2}}(1 - p_x^2 v^2)^{3/2}. \qquad \text{(B-5)}$$

This solution is exact for $p_x = 0$ and $p_x = \frac{1}{v}$, and therefore, I will refer to it as the 2-point solution (it fits exactly at two points). Figure B-2 shows a comparison between the exact solution of equation (B-1) (obtained numerically) and that given by equation (B-5), again for three sets of $\frac{X}{\tau}$. Clearly, this new curve of p_h better fits the exact solution than that given in Figure B-1. Although the percentage of error in p_h seems to be high, the corresponding error in the phase estimate (which is the key quantity used in the migration) is much lower because p_τ, as depicted in Figure 1, is rather insensitive to p_h, especially around the exact solution. In other words, the curvature of the phase function around its minimum is low. Such low curvature, according to equation (A-2), will result in a greater contribution in terms of amplitude. This translates to practically no error when it comes to actual geophysical applications.

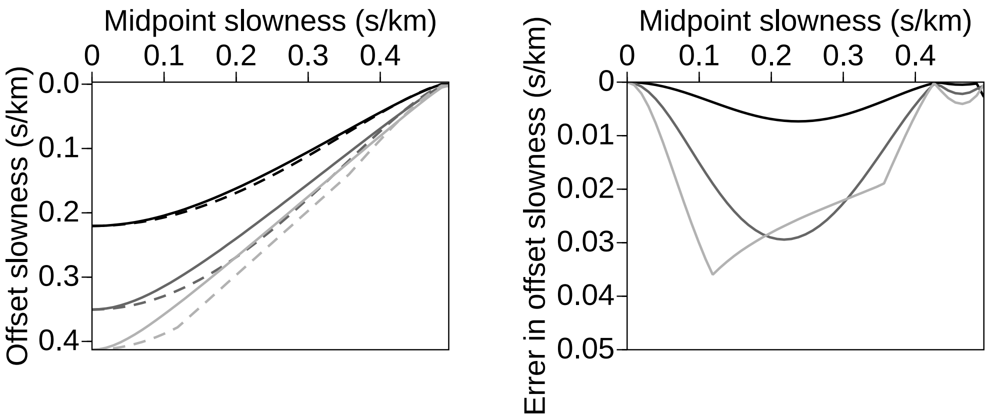

Figure B-2: Same as in Figure B-1, but with the analytical solution evaluated using the 2-point fitting of equation (B-5). tariq1-ph2eta0m [NR]

Let's find yet another exact solution, that is, the solution when p_s=0 ($p_x = p_h$). The reflector angular correspondence of this approximation depends on the offset. In this case, equation (B-1) reduces to

$$\frac{\partial T(p_h, v, \frac{X}{\tau})}{\tau \partial p_h} \,|_{p_h = p_{hs}} = \frac{p_{hs} v^2}{\sqrt{1 - 4 p_{hs}^2 v^2}} + \frac{X}{\tau} = 0. \tag{B-6}$$

with a solution for p_h given by

$$p_{hs} = \frac{\frac{X}{\tau}}{v\sqrt{4(\frac{X}{\tau})^2 + v^2}}. \tag{B-7}$$

To insure that p_h given by equation (B-5) has the value of p_{hs} as $p_x = p_h$, we must insert, some how, equation (B-7) into equation (B-5). This task is accomplished by forcing p_h, given by equation (B-5), to linearly equal p_{hs} at $p_x = p_h$, and, thus, equation (B-5) becomes

$$p_h = \frac{\frac{X}{\tau}}{v\sqrt{(\frac{X}{\tau})^2 + v^2}} (1 - p_x^2 v^2)^{3/2} [a(p_{hs}) p_x + b]. \tag{B-8}$$

The term between the square brackets is to insure this linear fit. To solve for a and b in equation (B-8), p_h must satisfy two conditions: (1) p_h should reduce to the form given by equation (B-3) for p_x=0, and this condition will result in $b = 1$. (2) p_h should reduce to the form given by equation (B-7) for $p_x = p_{hs}$. The second condition, after some mathematical manipulation, yields

$$a = \frac{1}{p_{h0}(1 - p_x^2 v^2)^{3/2}} - \frac{1}{p_{hs}}.$$

Therefore, p_h given by equation (B-8) is an exact solution of equation (B-1) at three points (p_x=0, $p_x = p_{hs}$, and $p_x = \frac{1}{v}$) and a good approximation, as demonstrated by Figure B-3, elsewhere. I will refer to this equation as the 3-point solution.

Figure B-3 shows p_h given by equation (B-8) next to the exact solution for p_h. Clearly, the three point fitting given by equation (B-8) resulted in a good approximation of p_h. The accuracy of this approximation will be better appreciated when we observe the low amount of errors in traveltime calculation induced by this approximation (i.e., Figure 3).

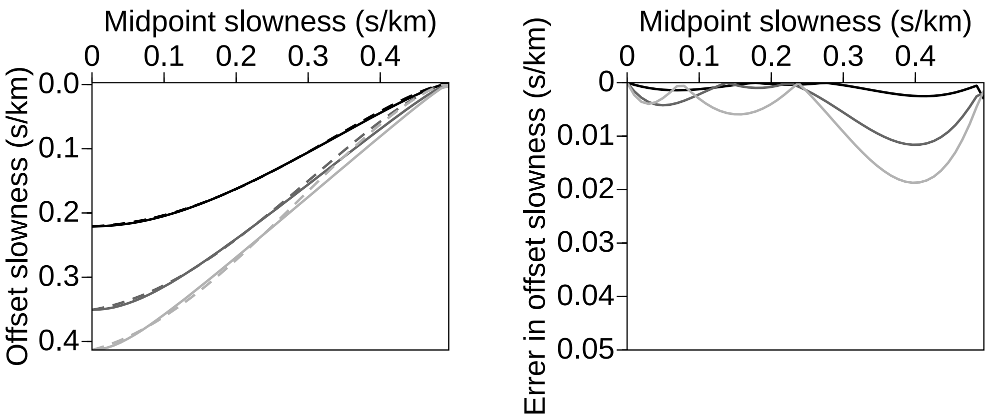

Figure B-3: Same as in Figure B-1, but with the analytical solution evaluated using the 3-point fitting of equation (B-8). tariq1-ph3eta0m [NR]

VTI homogeneous media

The time-processing operators in VTI media, as mentioned earlier, depend primarily on two parameters, $V_{\rm nmo}$ and η. This dependency becomes exact when the shear wave velocity (V_{S0}) is set to zero (Alkhalifah, 1997c). Setting $V_{S0} = 0$, although not practical for TI media, yields remarkably accurate kinematic representations. Errors due to this approximation, for practical VTI models, are kinematically, in a worse-case scenario, less than 0.5 percent, which is far within the limits of seismic accuracy. This acoustic approximation yields simplified equations, including a simplified dispersion relation. Because the vertical P-wave velocity does not have any significance in time-related processing in VTI media (Alkhalifah and Tsvankin, 1995), I will refer to $V_{\rm nmo}$ as the velocity and denote it by the symbol v to simplify comparisons with isotropic media. The zero-offset time-migration dispersion relation for VTI media, when V_{S0}=0, is given by

$$\cos\theta(t) = 1 - \frac{v^2 p_x^2}{1-2\eta v^2 p_x^2}$$

(Alkhalifah, 1997c). Based on this relation, the normalized DSR equation, for VTI media, has the form

$$\frac{T(p_x,p_h,v,\eta)}{\tau} = 0.5(\sqrt{1-\frac{(p_x+p_h)^2v^2}{1-2\eta v^2(p_x+p_h)^2}} + \sqrt{1-\frac{(p_x-p_h)^2v^2}{1-2\eta v^2(p_x-p_h)^2}}) + p_h\frac{X}{\tau}, \tag{B-9}$$

Clearly, for η=0, the above equations reduce to there isotropic counterparts. The stationary point (or points) satisfy the following relation

$$\begin{aligned}\frac{\partial T}{\tau\partial p_h} &= 0.5(\frac{(p_x-p_h)v^2}{[1-2\eta(p_x-p_h)^2v^2]^2\sqrt{1-\frac{(p_x-p_h)^2v^2}{1-2\eta v^2(p_x-p_h)^2}}} \\ &- \frac{(p_x+p_h)v^2}{[1-2\eta(p_x+p_h)^2v^2]^2\sqrt{1-\frac{(p_x+p_h)^2v^2}{1-2\eta v^2(p_x+p_h)^2}}}) + \frac{X}{\tau} = 0.\end{aligned} \tag{B-10}$$

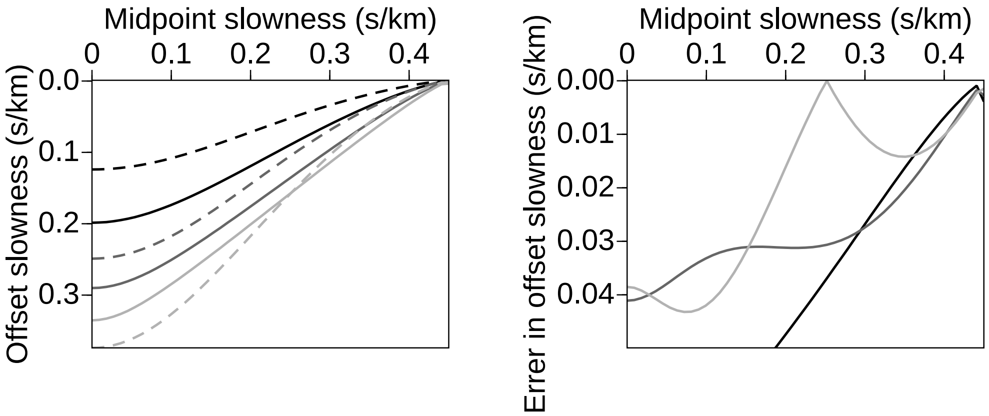

Figure B-4: Left: Values of p_h as a function p_x calculated numerically (solid curves), and calculated analytically (dashed curves) using equation (B-1). Right: The absolute difference between the two curves on the right. The medium is homogeneous and transversely isotropic with v=2.0 km/s and η=0.2.. The black curve corresponds to $\frac{X}{\tau}$=1.0 (km/s), the dark-gray curve corresponds to $\frac{X}{\tau}$=2.0 (km/s), and the light gray curve corresponds to $\frac{X}{\tau}$=3.0 (km/s). $\boxed{\text{tariq1-ph1eta2m}}$ [NR]

Following the same approach used in the previous sections for isotropic media, we set p_x=0, and as a result, equation (B-10) reduces to

$$\frac{p_h v^2}{(1-2\eta v^2 p_h^2)^3 \sqrt{1-\frac{p_h^2 v^2}{1-2\eta v^2 p_h^2}}} = \frac{X}{\tau}.$$

Squaring both sides and expanding in p_h, we get

$$8\eta^3 X^2(1+2\eta)y^4 - 4\eta^2 X^2(3+8\eta)y^3 + 6\eta X^2(1+4\eta)y^2 - [X^2(1+8\eta)+\tau^2 v^2]y + X^2 = 0,$$

where $y = p_h^2 v^2$. This is a quartic equation in y, which, although,it has analytical solutions, is best solved numerically. Considering either η or y (αp_h^2), or both, to be small, we can drop terms of y beyond the quadratic (perturbation theory; Bender and Orszag, 1978) , and as a result, the quartic equation reduces to

$$ay^2 + by + c = 0,$$

where

$$a = 6\eta X^2(1+4\eta),$$

$$b = -X^2(1+8\eta) - \tau^2 v^2,$$

and

$$c = X^2. \tag{B-11}$$

Because η can be small, as small as zero for isotropic media, I prefer to use the following form of solution of the quadratic equation:

$$y = \frac{2c}{-b \pm \sqrt{b^2-4ac}}$$

(Press et al., 1988). Thus,

$$p_{h0} = \frac{1}{v}\sqrt{\frac{2c}{-b \pm \sqrt{b^2-4ac}}}, \tag{B-12}$$

where the positive-sign root is used. The negative-sign root results in an imaginary p_h solution which is clearly not the solution we are looking for. Another, yet better, approximation is described in Appendix C using perturbation series as well as Shanks transformation. For η=0 (isotropic media), $a = 0$, and this equation reduces to equation (B-3), which is its isotropic counterpart. This is amazing considering we have dropped some terms in solving the quartic equation. Equation (B-11) is not the exact solution for horizontal reflectors in VTI media. However, as we will see bellow, it is a good approximation; better than similar approximations based on Taylors series expansion of traveltimes around the zero-offset point. Also, to insure we do not get imaginary roots for p_h, $b^2 - 4ac$ must be greater or equal zero. This results in the following condition that must be satisfied:

$$\tau^2 > [2\sqrt{6\eta(1+4\eta)} - (1+8\eta)]\frac{X^2}{v^2},$$

which corresponds to large offset-to-depth ratio. For practical values of $\eta (< 0.3)$, this condition is far within the typical mute zone. For example, if $v = 2$ km/s, $\eta = 0.3$, and $X = 3$ km, τ=1.14 s.

Expanding equation (B-10) using Taylors series, around p_h=0 ($p_x = \frac{1}{v\sqrt{1+2\eta}}$), and ignoring terms beyond the linear, yields

$$\frac{X}{\tau} - \frac{p_h v^2 [1 + 4\eta p_x^2 v^2 - 6\eta(1+2\eta) p_x^4 v^4]}{(1 - 2\eta p_x^2 v^2)^4 (\frac{1 - p_x^2 v^2 - 2\eta p_x^2 v^2}{1 - 2\eta p_x^2 v^2})^{3/2}} = 0. \tag{B-13}$$

As a result, the stationary point is given by

$$p_h = \frac{\frac{X}{\tau}}{v^2} \frac{(1 - 2\eta p_x^2 v^2)^4 (\frac{1 - p_x^2 v^2 - 2\eta p_x^2 v^2}{1 - 2\eta p_x^2 v^2})^{3/2}}{[1 + 4\eta p_x^2 v^2 - 6\eta(1+2\eta) p_x^4 v^4]}. \tag{B-14}$$

Again, I insert equation (B-11) in place of $\frac{\frac{X}{\tau}}{2v^2}$, and obtain

$$p_h = \frac{1}{v} \sqrt{\frac{2c}{-b \pm \sqrt{b^2 - 4ac}} \frac{(1 - 2\eta p_x^2 v^2)^4 (\frac{1 - p_x^2 v^2 - 2\eta p_x^2 v^2}{1 - 2\eta p_x^2 v^2})^{3/2}}{[1 + 4\eta p_x^2 v^2 - 6\eta(1+2\eta) p_x^4 v^4]}}. \tag{B-15}$$

where a, b, and c are given by equation (B-11). Equation (B-15) is exact for $p_x = \frac{1}{v\sqrt{1+2\eta}}$ ($p_h = 0$). However, unlike the isotropic medium case, equation (B-15) is an approximation at $p_x = 0$. [Recall that we dropped terms beyond the quadratic in equation (B-13).] Despite the approximation used at p_x=0, I will refer to this equation as the 2-point solution for VTI media.

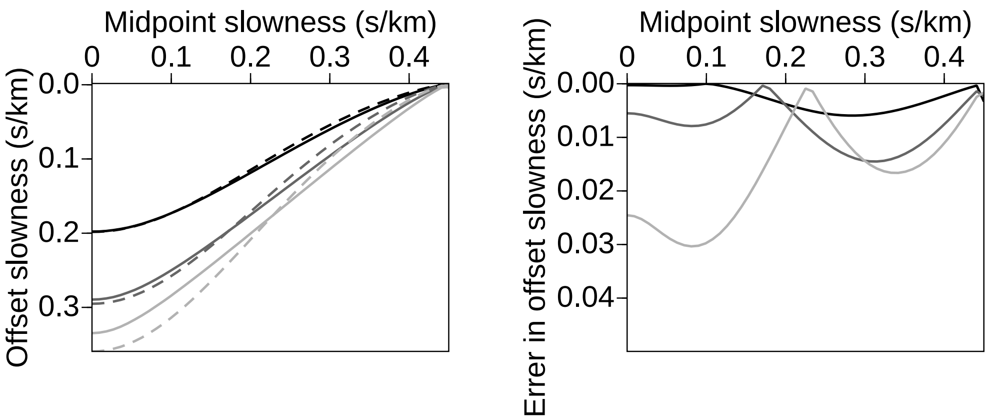

Figure B-5: Same as in Figure B-1, but with the analytical solution evaluated using the 2-point fitting of equation (B-15). tariq1-ph2eta2m [NR]

Figure B-5 shows p_h given by equation (B-15) and compares it with the accurate result calculated numerically from equation (B-10) for three sets of $\frac{X}{\tau}$. Despite the large non-hyperbolic moveout associated with horizontal events in such VTI media

(Alkhalifah, 1997b), the approximation at $p_x = 0$, which corresponds to a horizontal event, is rather good. Combine this with the fact that the phase [equation (B-9)] changes slowly as a function of (or rather insensitive to) p_h around the exact solution, the result is a good approximation of the phase for all p_x (slopes).

The accuracy of equation (B-15) can be further enhanced, as in the isotropic case, by fitting it to the exact solution for $p_x = p_h$; the angular correspondence of this equality depends on the offset-to-depth ratio. Following the same steps used to obtain the p_h for $p_x = 0$, including dropping terms beyond the quadratic in a similar quartic equation to that of equation (B-13), the stationary point is given by

$$p_{hs} = \frac{1}{v}\sqrt{\frac{2c}{-b \pm \sqrt{b^2 - 4ac}}}, \tag{B-16}$$

where

$$a = 96\eta X^2(1 + 4\eta),$$

$$b = -4X^2(1 + 8\eta) - \tau^2 v^2,$$

and

$$c = X^2.$$

Equatio (B-16)n has a stricter condition for its validity (that is avoiding imaginary roots) than that of equation (B-11). Specifically,

$$\tau^2 > 4[2\sqrt{6\eta(1 + 4\eta)} - (1 + 8\eta)]\frac{X^2}{v^2},$$

which correspond to double the time for the horizontal reflector solution fitting. For $v = 2$ km/s, $\eta = 0.3$, and $X = 3$ km, τ=2.28 s.

Again, inserting equation (B-16) into equation (B-15) requires solving two equations and, similar to the case of isotropic media, the solution is given by

$$p_h = p_{h0}\frac{(1 - 2\eta p_x^2 v^2)^4(\frac{1-p_x^2v^2-2\eta p_x^2 v^2}{1-2\eta p_x^2 v^2})^{3/2}}{[1 + 4\eta p_x^2 v^2 - 6\eta(1 + 2\eta)p_x^4 v^4]}[a(p_{h0})p_x + b], \tag{B-17}$$

where setting p_x=0 gives b=1 and setting $p_x = p_{hs}$ results in

$$a = \frac{1}{p_{h0}}\frac{1 + 4\eta p_x^2 v^2 - 6\eta(1 + 2\eta)p_x^4 v^4}{(1 - 2\eta p_x^2 v^2)^4(\frac{1-p_x^2v^2-2\eta p_x^2 v^2}{1-2\eta p_x^2 v^2})^{3/2}} - \frac{1}{p_{hs}}.$$

Figure B-6 shows the numerically-driven curves (solid ones) along with the analytical curves calculated using the 3-point fitting of equation B-17. The 3-point equation provides the best estimation to the exact solution for $\frac{X}{\tau}$.

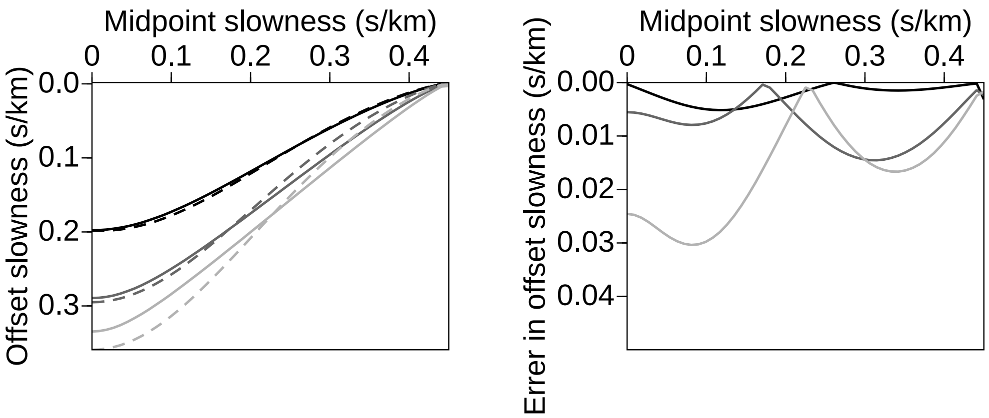

Figure B-6: Same as in Figure B-1, but with the analytical solution evaluated using the 3-point fitting of equation (B-17). $\boxed{\text{tariq1-ph3eta2m}}$ [NR]

APPENDIX C

BETTER STATIONARY-PHASE APPROXIMATIONS

Although previous approximations of p_h for horizontal reflectors in VTI media (Appendix B) yield adequate results, better approximations based on perturbation theory can further enhance the accuracy of the migration. The theory is based on expressing the solution in terms of power-series expansions of parameters that are expected to be small. As a result, higher power terms have smaller contributions, and as a result, they are usually dropped. The degree of truncation depends on the convergence behavior of the series. I will apply the perturbation theory to evaluate the stationary-phase solution at $p_x = 0$ and $p_x = p_h$ in VTI media.

In the case of $p_x = 0$, the stationary point solution p_h, as we saw earlier, satisfies

$$8\eta^3X^2(1+2\eta)y^4 - 4\eta^2X^2(3+8\eta)y^3 + 6\eta X^2(1+4\eta)y^2 - [X^2(1+8\eta)+\tau^2v^2]y + X^2 = 0, \tag{C-1}$$

where $y = p_h^2v^2$. Analytical solutions for this quartic equation in y exist. They are, however, complicated, and some of them actually do not exist ($\rightarrow \infty$) for η=0. Recognizing that both η and p_h can be small, we can drop terms beyond the quadratic, as done in Appendix B, and solve the resultant quadratic equation analytically. We can also benefit from fact that η can be small and use perturbation series, that is, apply a power-series expansion in terms of η. Unlike weak anisotropy approximations, the resultant solution yields good results even for strong anisotropy ($\eta > 0.5$). The key here is to recognize the behavior of the series for large powers of η using Shanks transforms. According to the perturbation theory (Bender and Orszag, 1978), the solution of equation (C-1) can be represented in a power-series expansion in terms of

η as follows

$$y = \sum_{i=0}^{\infty} y_i \eta^i, \tag{C-2}$$

where y_i are coefficients of this power series. For practical applications, the power series of equation (C-2) is truncated to n terms as follows

$$A_n = \sum_{i=0}^{n} y_i \eta^i. \tag{C-3}$$

The coefficients, y_i, are determined by inserting the truncated form of equation (C-2) (three terms of the series are enough here) into equation (C-1) and then solving for y_i, recursively. Because η is a variable, we can set the coefficients of each power of η separately to equal zero. This gives a sequence of equations for the y_i expansion coefficients. For example, y_0 is obtained directly from setting η=0, and the result corresponds to the solution for isotropic media. For large η, A_n converges slowly to the exact solution, and, therefore, yields sub-accurate results when used, even if we go up to A_{10}. Truncating after the second term (linear in η, A_1) is referred to as the weak anisotropy approximation. Using Shank transforms (Bender and Orszag, 1978), one can predict the behavior of the series for large n, and, therefore, eliminate the most pronounced transient behavior of the series (to eliminate the term that has the slowest decay). Following Shanks transform, the solution is evaluated using the following relation

$$y_s = \frac{A_2 A_0 - A_1^2}{A_2 + A_0 - 2A_1}.$$

After some tedious algebra, done using primarily the *Mathematica* program, p_h corresponding to horizontal events is given by

$$p_{h0} = \frac{1}{v}\sqrt{\frac{X^2\ (X^6 - 6\,v^2\,X^4\ (-1+\eta)\ \tau^2 + 3\,v^4\,X^2\ (3+4\,\eta)\ \tau^4 + 4\,v^6\,\tau^6)}{(X^2+v^2\,\tau^2)\ (X^6\ (1+2\,\eta) + 2\,v^2\,X^4\ (3+5\,\eta)\ \tau^2 + v^4\,X^2\ (9+44\,\eta)\ \tau^4 + 4\,v^6\,\tau^6)}}. \tag{C-4}$$

Unlike equation (B-12), which corresponds to the solution of the quadratic truncation of equation (C-1), equation (C-4) is valid for all practical models. No validity conditions are required here.

The same steps used above to evaluate p_h for $p_x = 0$ is used for the case $p_x = p_h$ ($p_s = 0$), and, as a result,

$$p_{hs} = \frac{1}{v}\sqrt{\frac{X^2\ (16\,X^6 - 24\,v^2\,X^4\ (-1+\eta)\ \tau^2 + 3\,v^4\,X^2\ (3+4\,\eta)\ \tau^4 + v^6\,\tau^6)}{(4\,X^2+v^2\,\tau^2)\ (16\,X^6\ (1+2\,\eta) + 8\,v^2\,X^4\ (3+5\,\eta)\ \tau^2 + v^4\,X^2\ (9+44\,\eta)\ \tau^4 + v^6\,\tau^6)}}. \tag{C-5}$$

Now, we insert the new definitions of p_{h0} and p_{hs} into equation (B-17):

$$p_h = p_{h0}\frac{(1-2\eta p_x^2 v^2)^4 (\frac{1-p_x^2 v^2 - 2\eta p_x^2 v^2}{1-2\eta p_x^2 v^2})^{3/2}}{[1+4\eta p_x^2 v^2 - 6\eta(1+2\eta)p_x^4 v^4]}[a(p_{h0})p_x + 1], \tag{C-6}$$

where

$$a = \frac{1}{p_{h0}} \frac{1 + 4\eta p_x^2 v^2 - 6\eta(1+2\eta)p_x^4 v^4}{(1 - 2\eta p_x^2 v^2)^4 (\frac{1 - p_x^2 v^2 - 2\eta p_x^2 v^2}{1 - 2\eta p_x^2 v^2})^{3/2}} - \frac{1}{p_{hs}}.$$

Figure C-1 shows a comparison between the exact p_h solution of equation (B-1) (obtained numerically) and that given by equation (C-6) as a function of p_x for three sets of $\frac{X}{\tau}$. The absolute difference between the two solutions is also displayed. Clearly, results, obtained using the modified equation, are far superior to the ones obtained in Appendix B for VTI media.

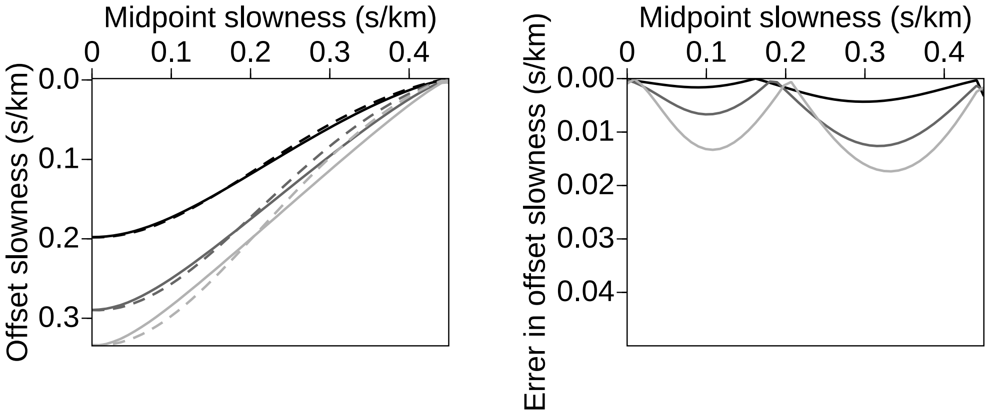

Figure C-1: Left: Values of p_h as a function of p_x calculated numerically (solid curves), and calculated analytically (dashed curves) using equation (C-6). Right: The absolute difference between the two curves on the left. The medium is homogeneous and isotropic with v=2.0 km/s. The black curve corresponds to $\frac{X}{\tau}$=1.0 km/s, the dark-gray curve corresponds to $\frac{X}{\tau}$=2.0 km/s, and the light gray curve corresponds to $\frac{X}{\tau}$=3.0 km/s. tariq1-ph3sheta2m [NR]